PRECIOUS METAL ENRICHMENT AT THE MYRA FALLS VMS DEPOSIT, BRITISH COLUMBIA, CANADA

D. MARSHALL
Earth Sciences, Simon Fraser University, Burnaby, BC, V5A 1S6, Canada
C-A. NICOL
Earth Sciences, Simon Fraser University, Burnaby, BC, V5A 1S6, Canada
R. GREENE
Earth Sciences, Simon Fraser University, Burnaby, BC, V5A 1S6, Canada
R. SAWYER
Nyrstar Mining, Campbell River, BC, V9W 5E2, Canada
A. STANSELL
Nyrstar Mining, Campbell River, BC, V9W 5E2, Canada
R. EASTERBROOK
Coeur Mining, Chicago, IL 60603, USA

Abstract

Gold, present as electrum, in the Battle Gap, Ridge North-West, HW, and Price deposits at the Myra Falls mine, occurs in late veinlets cutting the earlier VMS lithologies. The ore mineral assemblage containing the electrum comprises dominantly galena, tennantite, bornite, sphalerite, chalcopyrite, pyrite and rare stromeyerite is defined as an Au-Zn-Pb-As-Sb association. The gangue is comprised of barite, quartz, and minor feldspathic volcanogenic sedimentary rocks and clay.

Deposition of gold as electrum in the baritic upper portions of the sulphide lenses occurs at relatively shallow water depths beneath the sea floor. Primary, pseudosecondary, and secondary fluid inclusions, petrographically related to gold, show boiling fluid inclusion assemblages in the range of 123 to 173 ˚C, with compositions and eutectic melt temperatures consistent with seawater at approximately 3.2 wt% NaCl equivalent. The fluid inclusion homogenization temperatures are consistent with boiling seawater corresponding to water depths ranging from 15

 doi:10.20944/preprints201809.0151.v1

to 125 metres. Slightly more dilute brines corresponding to salinities of approximately 1 wt% NaCl indicate that there is input from very low-salinity brines, which could represent a transition from subaqueous VMS to epithermal-like conditions for precious metal enrichment, mixing with re-condensed vapour, or very low-salinity igneous fluids.

INTRODUCTION

The Myra Falls (MF) polymetallic volcanogenic massive sulphide (VMS) deposit is located on Vancouver Island within a series of middle to late Devonian Sicker group volcanogenic rocks (Fig. 1). It best fits a Kuroko-type or Bimodal-Felsic model [1]. While parts of the mine average above 4 grams of gold per metric ton of ore, the overall proven mineral reserves for gold grade for the entire mining operation may be a bit lower averaging 1.60 and 1.69 g/t for 2017 and 2016 respectively. Precious metal production at Myra Falls is of significant economic importance, with annual production of approximately 6,000 and 240,000 troy ounces of gold and silver respectively [2].

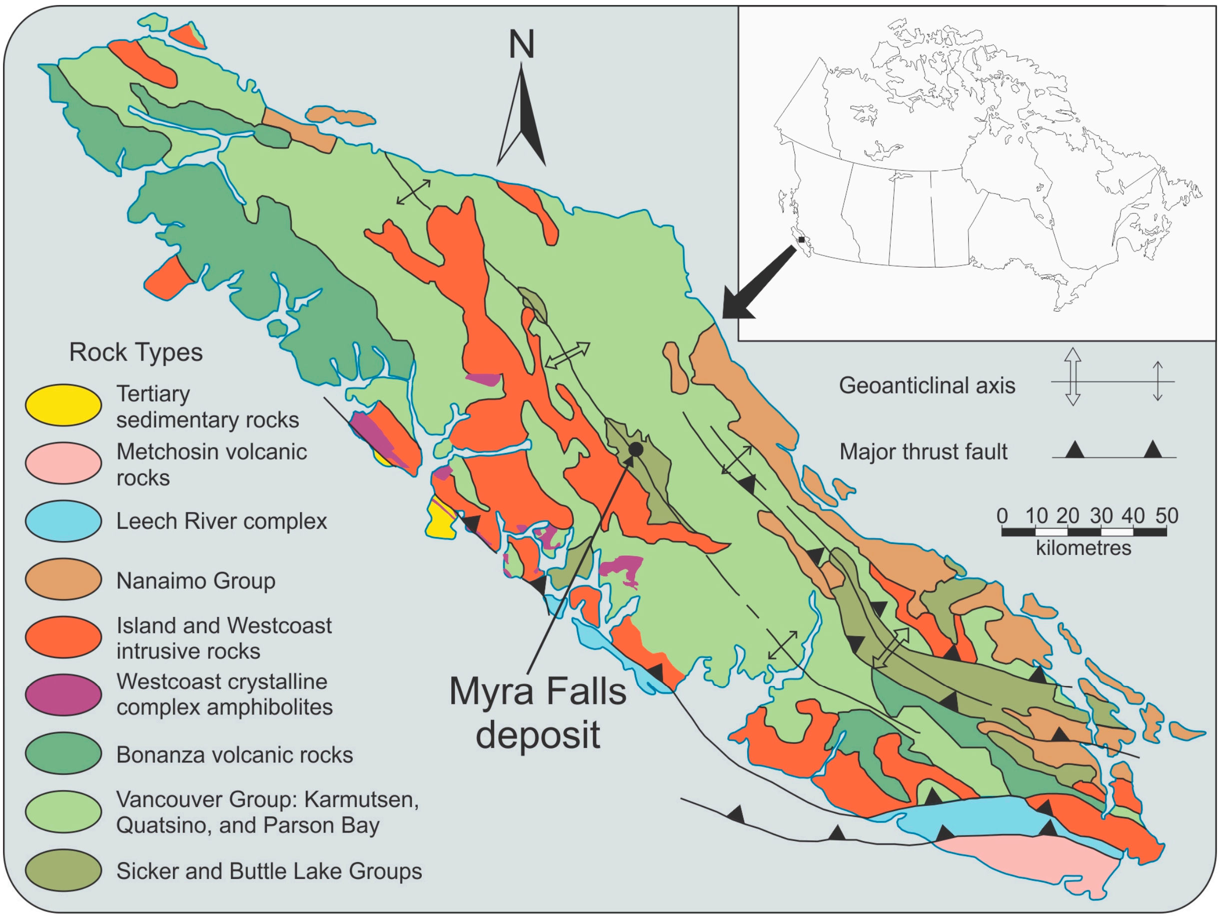

Figure 1: Regional geological map showing the major lithological units at the Myra Falls mine. Inset figure shows the location of the mine within Canada.

Gold has four different occurrences in VMS deposits: i) Au-Zn-Pb-Ag-Sb barite association, ii) Au-Cu-Bi-Co association, iii) Au-enriched, base metal-poor massive pyrite, iv) Au-rich deposits that have been supergene altered [3]. The Au-Zn-Pb-Ag-Sb barite and Au-Cu associations are the most well documented, having been observed in both ancient VMS deposits [4] and active black smoker deposits [5].

The Au-Zn-Pb-Ag-Sb barite assemblage is generally found concentrated near the top of massive sulphide lenses, with significant Au concentrations present in the overlying massive barite zones [3], often associated with siliceous cap rocks. Enrichment of Au at the top of the deposit is due to metal zonation refinement by sustained circulation of hydrothermal fluids through the underlying volcanic pile [4]. Gold is leached from the base and center of the massive sulphide lens and then reprecipitated at the top of the deposit. Au located in the massive barite zone often lacks the close association with pyrite [6]. Gold in the upper portions of the deposit is believed to be transported predominantly by thio complexes (especially $Au(HS)_2^-$) in low temperature (150-250 °C), near-neutral (pH>3.5) hydrothermal fluids, with lesser amounts of transport via gold chloride complexes. Deposition occurs when these fluids mix with seawater, causing oxidation, an increase in pH, and most importantly, a decrease in a_{H2S}. The activity of H_2S is mainly reduced by deposition of metallic sulphide minerals and dilution [4]. Feldspar-bearing alteration assemblages, possibly containing albite and celsian gangue, are commonly associated with the Au-Zn-Pb-Ag-Sb barite assemblage [3]. Although gold at MF also occurs to a lesser extent in Au-enriched, base metal-poor massive pyrite lenses, the Au-Zn-Pb-Ag-Sb association is the dominant mode of gold occurrence at MF and is the focus of this study.

REGIONAL AND LOCAL GEOLOGY

Preprints (www.preprints.org) | NOT PEER-REVIEWED | Posted: 10 September 2018 doi:10.20944/preprints201809.0151.v1

The Myra Falls deposit is located within the Paleozoic Sicker Group, which constitutes the basement of the Wrangellia terrane and Vancouver Island [7]. The Sicker Group is overlain unconformably by the Permian Buttle Lake Group limestones and younger rocks. Rocks of the Wrangellia terrane are generally metamorphosed to greenschist facies, with some amphibolite-facies contact-metamorphic zones near the Jurassic Island intrusive rocks [8].

The Sicker Group volcanic rocks are exposed in several anticlinal zones on Vancouver Island, such as the Buttle Lake, Cowichan, Nanoose and West Coast uplifts [7,8]. The Sicker Group is divided into four formations. The Price Formation is stratigraphically lowest and the footwall of the HW and Battle orebodies (Fig. 2). It consists of andesitic volcanic and volcaniclastic rocks that were deposited directly on the seafloor. The contact with the overlying Myra Formation, host to the orebodies, is a transition from andesitic volcanic to rhyolitic volcaniclastic rocks.

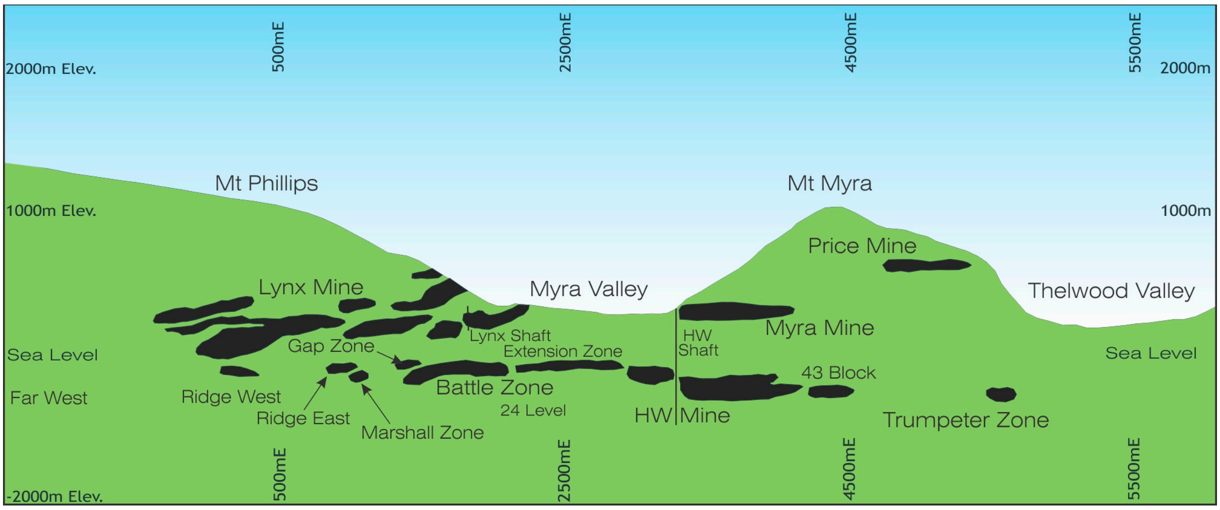

Figure 2. Schematic cross section showing the relative positions of the different ore bodies within the Myra Falls mine (after [9]).

The Myra Formation is a succession of rhyolitic, andesitic and basaltic volcanic and sedimentary rocks. The HW and battle deposits are found within its basal unit, the HW horizon. The HW horizon consists of coarse-grained rhyolitic volcaniclastic rocks, sandstones and mudstones overlain by massive porphyries. The HW and Battle orebodies are mostly found in volcaniclastic rocks near the base of the HW horizon. They are massive to semimassive tabular sulphide lenses, with main ores of chalcopyrite, sphalerite, pyrite and galena. Some bornite and tetrahedrite, as well as accessory chalcocite, colusite and gold are also present. The HW horizon also hosts zones of semimassive sulphides above the Battle and HW deposits. These are high in sphalerite, galena and barite, but low in pyrite. The sulphide lenses are zoned vertically and laterally and accompanied with silicification of the host rocks. Overlying the HW horizon are thick hangingwall andesites, which are conformably overlain by a unit of volcaniclastic, felsic volcanic and sedimentary rocks. The Lynx-Myra-Price orebodies are hosted within this unit.

The Myra Formation is overlain by the Thelwood Formation, which is a laminated mudstone interbedded with volcaniclastic rocks and mafic sills. The Thelwood Formation is overlain conformably by the Flower Ridge formation, a package of amygdaloidal basaltic flows and volcaniclastic rocks, tuffaceous siltstones, wackes and argillites [8].

The Myra Falls area was affected by five separate deformation events, which have influenced the formation and distribution of the orebodies. First, pre-Permian event D_1 caused northwest-trending folding [7]. Early to Mid-Jurassic [7] folding event D_2 resulted in localized shear zones and reactivated F_1 folds [8]. Steep, conjugate strike-slip faults and bedding-parallel thrust faults and shears resulted from event D_3 [7,8], normal faults from event D_4, and large thrust faults and steep, west- to west-northwest-striking sinistral strike-slip faults from event D_5 [8].

Paleoseafloor reconstructions following the top of the Price andesites showed that the HW and Battle deposits formed in small basins in a northwest-trending ridge. These basins were constrained by growth faults [7,8], which acted as conduits for fluid migration [8].

 doi:10.20944/preprints201809.0151.v1

ANALYTICAL METHODS

Sampling

Given the 4 possible modes of gold/electrum occurrence in VMS deposits, samples were taken from a number of locations within the mine or from drill core where visible gold occurred. These samples were selected to optimize the study of petrographic relationship between gold, other ore, gangue, and alteration minerals. Areas within the mine sampled either from active stopes, existing samples or drill core include: Battle Gap, Ridge Northwest, HW North Slope, HW South Flank, HW stringer zone, Marshall, and Price (Fig. 2).

Electron microprobe mineral composition data

Selected doubly polished plates and polished thin sections containing gold compounds had in-situ electron microprobe analysis of the electrum. Electron microprobe analyses of electrum were performed at Carleton University using an automated 4 spectrometer Camebax MBX electron probe using the wavelength dispersive x-ray analysis method (WDX). Operating conditions were: 15 kilovolts (kv) accelerating potential and a beam current of 20 nano-amperes (nA). Counting times were up to 50 seconds or 40,000 accumulated counts. X-ray lines were chosen to minimize or eliminate possible elemental interferences. Raw x-ray data were converted to elemental weight % via the Cameca PAP matrix correction program. For the elements considered, the following standards, X-ray lines and crystals were used: $Au_{80}Ag_{20}$, Au Lα; $Ag_{80}Au_{20}$, Ag Lα; Chalcopyrite, Cu K α; Stibnite, Sb Kα; Cinnabar, Hg Kα

.*Raman spectroscopic analyses*

Raman identification of the accidental inclusions (minerals) within fluid inclusions was performed on a Renishaw inVia Raman spectrometer equipped with a 200 mW 785 nm laser and Olympus BX41 optical microscope. Spectra were collected from 500 to 3000 cm^{-1} in nonconfocal mode at room temperature. Areas of the individual gas peaks were parsed for gas abundances for CO_2, CH_4, N_2, and H_2S and none of these gases were found in any of the inclusions analysed in this study.

Fluid inclusion microthermometric measurements

For this study, 46 primary fluid inclusions hosted in quartz or barite in textural equilibrium with gold-bearing veins were targetted. Initial petrographic work was completed in order to identify different fluid inclusion assemblages in both quartz and barite. Fluid inclusion measurements were performed with a Linkam THMS-G 600 heating-freezing stage attached to an Olympus BX51 microscope equipped with 5, 10, 50 and 100x long working distance Olympus objectives. The stage is capable of measurements in the range of -190 to +400 ˚C. Prior to collecting the heating and cooling measurements the stage was calibrated with two synthetic fluid inclusion standards. The first yields phase transitions for pure H_2O at 0.0 and 374.1 °C. The second standard comprises H_2O-CO_2 fluid inclusions and is used to calibrate the stage at -56.6 °C to the melting of solid CO_2. The stage was periodically tested against the standards and results were always within ±0.2 ˚C for the two low temperature phase transitions and within ± 2.0 ˚C for the higher temperature phase transition.

GOLD VEINLET PETROLOGY

This study initially comprised the petrographic analysis of 93 samples. From these samples 14 containing gold in polished thin section were specifically targeted to determine mineral assemblages pre- and syn-gold mineralization. In the bulk of our samples, gold occurred in thin anastomosing to discontinuous veinlets (Fig. 3). Paragenesis for the deposit is complicated by numerous volcanic depositional events and by numerous deformational and subsequent alteration events [8]. However, the gold-bearing veinlets are very late in the deposit paragenesis and cross cut all of the typical sub- and seafloor sulphide mineralization associated with VMS deposits [1] including barite/silica cap rocks [8,10]. Gold grains, ranging up to 4 mm in size, are commonly visible in the veinlets, and contemporaneous with quartz, barite, sphalerite, galena, bornite, tennantite, chalcopyrite, pyrite and rarely stromeyerite, covellite, chalcocite, acanthite, and native silver. Grain sizes for the veins sulphides, barite, quartz, and tennantite ranged up to 1 cm. The wall rock to the veinlets are typical VMS assemblages comprising variable amounts of feldspars, quartz, sulphides, minor sulphosalts, chlorite, epidote, tremolite, clays, and barite. Barite is very common in the wall rock to the veinlets, and crystals may range up to 2.5 cm. Alteration of the wall rock proximal to the veins is generally silicification and relicts and pseudomorphs of barite are present. Generally, there is an alteration halo of quartz and silicification surrounding the veinlets (Fig. 3). The barites are often growth-zoned and also display relict crack seal trails of fluid inclusions. In some cases, silicification of the barite preserves the growth zones and crack seal textures, while in other samples crack seal textures occur in the silicified wall rock and quartz alteration haloes.

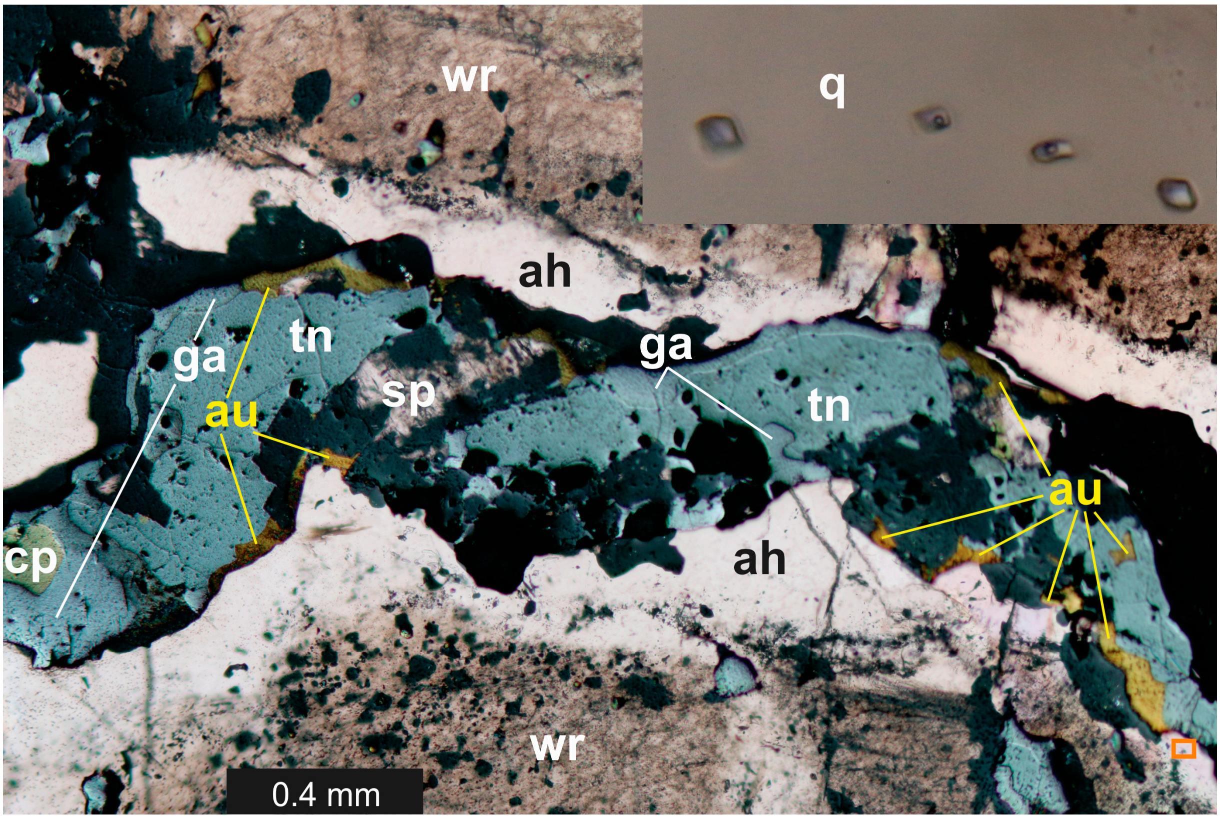

Figure 3. Composite photomicrographs of the alteration halo surrounding the gold-bearing veinlets and fluid inclusions. The main image, taken under simultaneous plane-polarized transmitted and reflected light, shows the barite-rich wall-rock (wr) and quartz dominated alteration halo (ah) surrounding the veinlet. The veinlet assemblage comprises tennantite (tn), galena (ga), sphalerite (sp), chalcopyrite (cp), and gold/electrum (au). The inset image shows the magnified region delineated by the orange rectangle, in plane-polarized light, comprising a trail of "boiling" pseudosecondary two-phase (liquid + vapour) fluid inclusions hosted within a quartz (q) crystal lining the walls of the veinlet. The central two fluid inclusions are from population P1L represent the liquid portion of the boiling fluid, while the outer two fluid inclusions are from population P1V and represent the conjugate vapour inclusions of the boiling system. Sample RG14-21B, inset field of view is approximately 50 microns wide.

The gold/electrum at Myra Falls is dominantly Au. Silver contents range throughout the deposit from approximately 30 to 35 wt% Ag. There are trace amounts of copper, with antimony and mercury below detection limits (Table 1). Nugget effect greatly dictates local Au grades, with electrum generally ranging from micron sized to a few millimetres and averaging less than a millimetre. The electrum is generally inclusion free, with occasional inclusions of quartz, barite, tennantite, sphalerite, and galena.

Preprints (www.preprints.org) | NOT PEER-REVIEWED | Posted: 10 September 2018 doi:10.20944/preprints201809.0151.v1

Table 1. Electron microprobe (wt%) data for electrum

Sample RG14-29	Au	Ag	Cu
Spot-1	67.823	31.906	0.028
-2	69.042	31.43	0.044
-3	67.345	32.004	0.014
-4	65.096	33.832	0.026
-5	67.409	33.246	0.009
-6	67.292	31.762	0.016
-7	68.237	31.479	0.001
-8	67.585	32.114	0.017
-9	68.45	31.001	0.009
-10	70.383	29.243	0.042
-11	68.002	31.503	0.028
-12	70.523	29.176	0.047

FLUID INCLUSIONS

Thirty-one doubly polished plates were examined in this study. A great deal of effort was expended to produce doubly polished plates with visible gold. Of the 31 samples, only 7 with visible gold survived the grinding and polishing process. This fluid inclusion study concentrated exclusively on the fluid inclusions petrographically related to the gold veinlets and the associated alteration halos. The fluid inclusions measured were hosted in the quartz or barite of the veinlets or their associated alteration haloes. Reconnaissance work on the larger number of samples revealed two populations of fluid inclusions: Population one (P1) is comprised of low-salinity two-phase liquid and vapour (L+V) fluid inclusions (FIs) and a more-rarely observed second population (P2) comprised of three-phase FIs. P2 is represented at room temperature by an aqueous phase, carbonic liquid and vapour phases. Both populations were identified in an earlier study [10], while a later study [8] only reported P1. Our observations for the P2 FIs concur with the earlier study of Barrett and Sherlock [10] that the origin of these inclusions is unclear and they are not representative of the overall hydrothermal system, and definitely not related to the precipitation of gold in the gold-bearing veinlets, thus no further study of the P2 fluids was pursued. Although both earlier studies reported primary, pseudosecondary, secondary, and indeterminate P1 fluid inclusions relative to base-metal VMS-type mineralization, the exact timing of these fluids relative to the late gold-bearing veinlets of this study is unclear. Our study indicates that the gold-bearing veinlets are late in the paragenesis of the deposit, occurring at lower temperatures, thus shallower water depths, than previously reported for the Myra Falls deposit.

P1 has been studied as Fluid Inclusion Assemblage (FIAs) permitting the interpretation of individual FIAs as contemporaneous [11]. Additionally, P1 is subdivided into mixtures of a two end member system ranging from vapour-dominant (P1V) FIs to the more prevalent liquid-

dominant (P1L) FIs. FI sizes range up to 12 microns in length, but average 4 microns. Due to the small size of the FIs, it was not possible to measure ice melting or liquid homogenization temperatures in the P1V end members. The presence of both liquid- and vapour-rich FIs within the same FIA is strong, but not conclusive evidence, of boiling. Further evidence to support our interpretation of boiling is presented below based on fluid compositions and specific formational models for VMS deposits. Phase observations in the P1L FIs are shown in Table 2. In general, the freezing behaviour upon cooling from room temperature results in the nucleation of ice between -42.3 to -28.3 °C. No further phase changes are observed upon cooling to -140 °C. In most cases the bubble disappears upon ice nucleation, with the vapour likely residing in the many cracks within the ice, occasionally, some vestiges of the bubble remain visible in the ice. Ice nucleation generally imparts a darkening to the FIs, and this is interpreted as light refraction at ice-vapour interfaces within the inclusion. Heating of the FIs from -140 °C results in first melting temperatures over the range -28.1 to -21.5 °C. This is marked by the disappearance of the darkening due to liquid replacing vapour in the cracks within the ice. Further heating results in final ice melting temperatures over the range -3.4 to -0.7 °C. Continued heating results in a gradual decrease in the vapour bubble volume until total homogenization into the vapour over the temperature range 119.5 to 172.8 °C. The microthermometric data for all the FIAs hosted in barite and quartz are shown in figure 4. Measurement of the ice melting temperatures was complicated by the presence of hydrohalite ($NaCl \cdot 2H_2O$), which is metastable above the melting temperature and prevents reappearance of the vapour bubble. The vapour phase was commonly metastably absent and difficult to impossible to nucleate in a number of fluid inclusions despite extended periods of freezing in liquid nitrogen or cooling in a refrigerator for days.
Femtosecond-laser excitation has proven useful in nucleating meta-stable vapour bubbles in some fluid inclusions [12], but was deemed beyond the scope of this study as the ice melting

Preprints (www.preprints.org) | NOT PEER-REVIEWED | Posted: 10 September 2018 doi:10.20944/preprints201809.0151.v1

temperatures could be measured in the absence of the vapour phase in some of our larger fluid inclusions, and was consistent with fluid inclusions within the same FIAs, that were able to nucleate vapour bubbles. Fluid inclusions in barite were especially affected by the absence of the vapour bubble, as it hinders ice melting measurements in small fluid inclusions where the ice itself is not readily visible.

Table 2: Microthermometric measurements on the pseudsecondary and secondary fluid inclusionsin quartz and barite

Chip / Flinc#	**eutectic**	**Tm ice**	**Th total**
RG14-21B-1-1-1	nv	-2.0	158.2
RG14-21B-1-2-1	nv	-2.0	169.6
-2	nv	-2.0	167.8
RG14-21B-1-3-1	nv	-2.2	145.3
-2	nv	-2.2	164.7
RG14-21B-1-4-1	nv	-1.9	152.0
-2	nv	-1.9	145.2
RG14-21B-1-5-1	-21.5	-1.8	158.7
-2	nv	-0.7	172.8
-4	-21.6	-2.3	148.9
-5	-25.2	-1.5	155.4
-6	-24.7	-1.7	157.2
RG14-21B-1-6-1	nv	-2.4	145.7
-2	nv	-2.4	156.1
-4	nv	-3.4	143.6
-5	nv	-3.4	150.5
-7	nv	-2.5	169.9
-8	nv	-2.4	159.8
RG14-21B-1-7-2	nv	-2.5	123.1
-3	-28.1	-3.3	127.2
-4	nv	-2.5	119.5
RG14-21B-2-1-1	-25.6	-2.0	130.5
RG14-21B-2-2-1	-24.0	-2.5	140.8
RG14-21B-2-3-1	nv	-1.2	144.5
-3	nv	-2.2	142.0
-6	nv	-1.1	145.9
RG14-21B-2-4-4	-22.6	-2.0	127.8
RG14-21B-2-5-1	nv	-2.3	123.8
-2	-23.5	-2.1	134.3
-3	nv	-2.3	135.1
RG14-21B-2-6-1	-22.5	-2.6	138.0
-2	nv	-2.6	141.0
RG14-33B-5-1-1	nv	-1.9	150.9

All temperatures reported in degrees Celsius, eutectic=ice melting eutectic temperature, Tm ice=Ice melting temperature, Tm ha=halite melting/dissolution temperature, Th total=vapour homogenization temperature into the liquid, nv=not visible, *italics* = barite hosted fluid inclusion, **bold** = pseudosecondary fluid inclusion, ***bold-italics*** = primary fluid inclusion

Preprints (www.preprints.org) | NOT PEER-REVIEWED | Posted: 10 September 2018 doi:10.20944/preprints201809.0151.v1

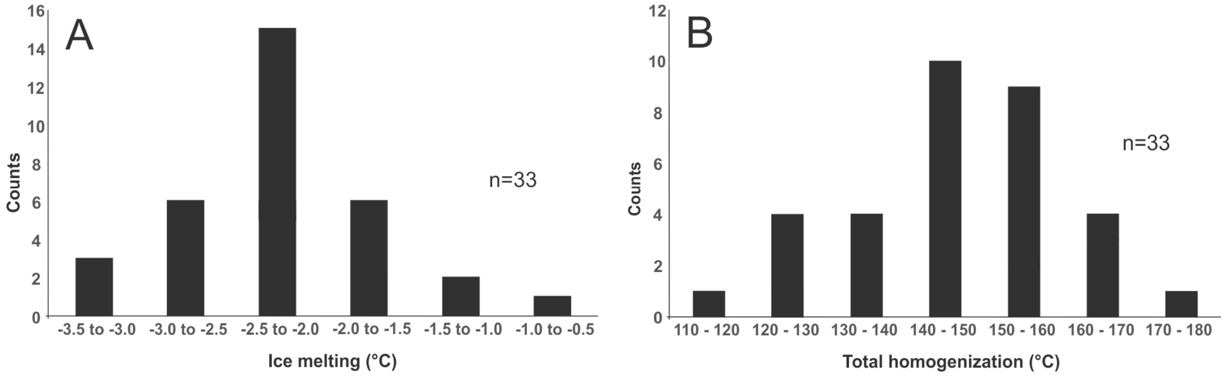

Figure 4. Histograms of the ice-melting (A) and total homogenisation (B) temperatures for the primary, secondary, and pseudosecondary two-phase (liquid + vapour) fluid inclusions (Table 2).

 doi:10.20944/preprints201809.0151.v1

MODEL FOR PRECIOUS METAL DEPOSITION

The primary, pseudosecondary, and secondary FIs related to the gold veinlets and associated alteration haloes (Fig. 3) yield salinities in the range -3.4 to -0.7 °C, corresponding to salinities of 1.2 to 5.6 wt % NaCl equivalent [13]. These salinities overlap with the theoretical salinities for seawater at approximately 3.2 wt % NaCl equivalent and eutectic temperatures (Table 2) are also consistent with published seawater compositions and microthermometric data [14,15]. Homogenization temperature range from 119.5 to 172.8 °C and have been plotted on the depth vs. boiling curve (Fig. 5) for seawater [16]. We reiterate that the FIAs show strong petrographic evidence of boiling and thus the measured FIs are consistent with seawater boiling at water depths of 15 to 125 metres. This model of gold precipitation at very moderate depths and pressures is consistent with the gold-bearing veinlets being one of the last events in the VMS formation, as the thicknesses of the volcanic sequences increase, bringing the sea-water volcanic rock interface to shallower and shallower water depths. Interestingly, the gold-bearing veinlets and associated alteration haloes, although generated by boiling seawater at shallow water depths, could occur at the seawater-rock interface or below to a maximum hydrostatic pressure corresponding to water depths listed above. Additionally, there is no reason that the gold-bearing veinlets could not occur in the near-shore terrestrial environment at depth within heated saltwater intrusions into the terrestrial meteoric water table (Fig. 6), as the volcanic system emerges from the sub-aqueous to the sub-aerial environment and show transitional features, such as fluid inclusion salinities slightly less than seawater salinities. This mixing of seawater with non-saline meteoric groundwater would produce diluted seawater brines and mark the transition from a VMS to an epithermal environment [18].

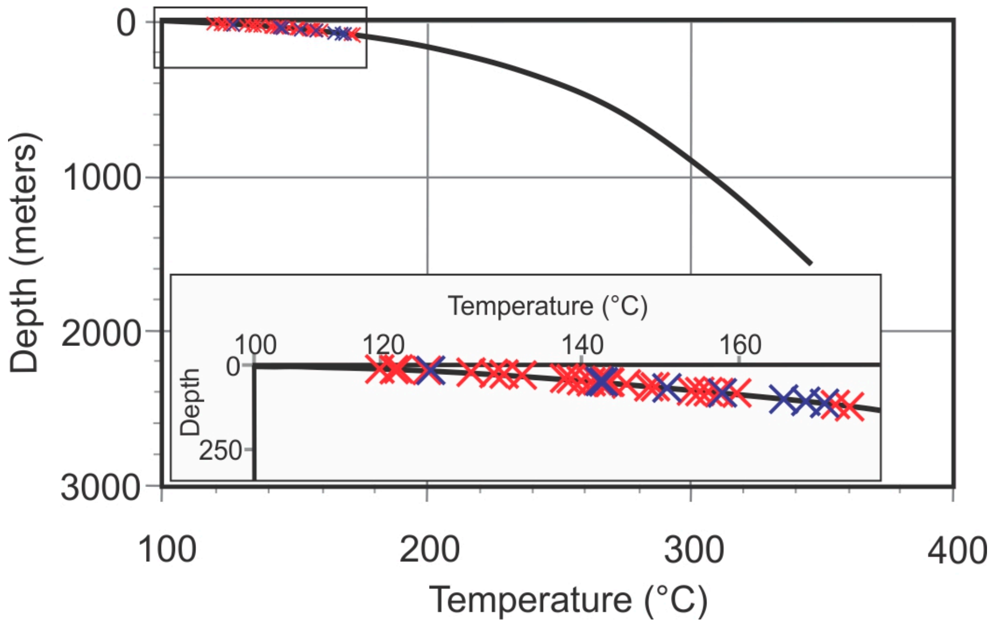

Figure 5. Temperature versus water depth boiling curve for seawater. Fluid inclusion homogenisation temperatures (Table 2) superimposed on the seawater boiling curve data from [16]. The expanded inset shows homogenization temperatures are consistent with boiling

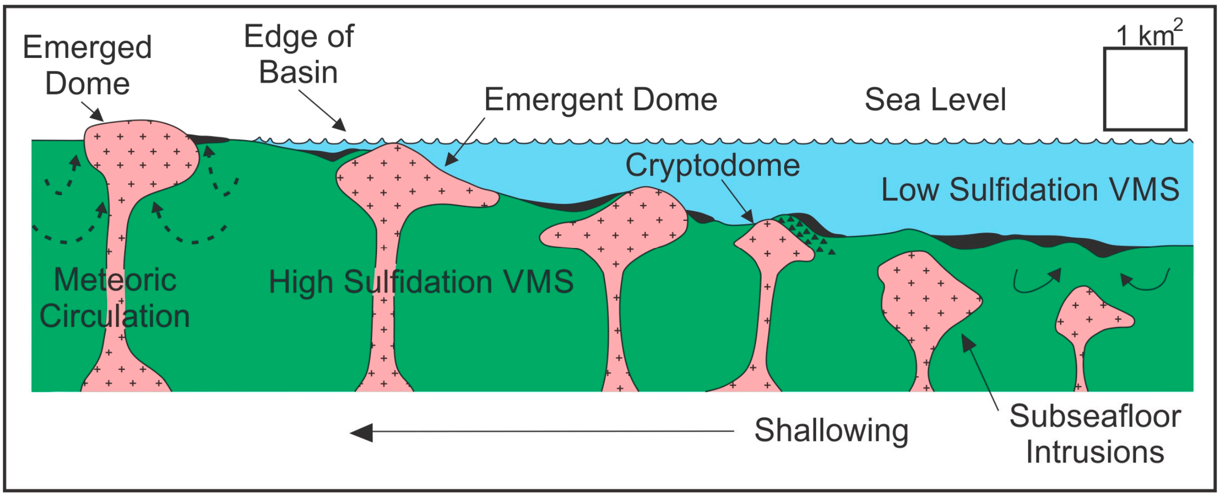

Figure 6. Schematic of volcanic rocks (green), subvolcanic intrusions (pink) and massive sulphides (black) of a VMS system evolving from seawater dominated circulation cells in the sub-aqueous environment to the epithermal environment dominated by meteoric water circulation cells (dashed curves). Modified from [17]. water

DISCUSSION AND CONCLUSIONS

This model of seafloor or sub-seafloor boiling, veining and gold deposition is consistent with previous research into gold in VMS systems [5,19,20], with gold concentration occurring via a process of seawater interacting with thick volcanic sequences of massive sulphides via cooling and/or boiling, increasing the relative solubility of gold in the fluid until reaching saturation and precipitation as per Hannington and Scott [5]. This is also consistent with the mineralogy observed within the veinlets and associated alteration haloes being enriched in tennantite, bornite, and barite typical of more sulphur-poor or oxygen-rich fluids.

This shallow-water model for gold precipitation may initially seem contradictory to the greater water depths formerly proposed for the Myra Falls VMS deposit [7,8,10]. However, we deem the two interpretations complementary, as the initial volcanic sequences, that later become host-rock to the gold-bearing veinlets are deposited earlier at greater water depths, with gold precipitation occurring later in the sequence, as the system is uplifted via tectonics related to arc formation in an emergent arc system similar to Kuroko and other Japanese deposits. This may also explain the dichotomy of proposed water depths for some other deposits such as Eskay Creek ranging from shallow to sub-aerial [21] to over 1500 meters [22].

As discussed previously, there is also some gold enrichment in pyrite-rich horizons in the Myra Falls system. It is presently unclear as to whether a model of nascent gold-bearing veinlet fluids, perhaps active along grain boundaries with fluid flow rates insufficient to generate specific veinlets and alteration, may be responsible for gold enrichment in the pyrite horizons. However, the lack of visible gold, barite, tennantite, bornite and silica in these horizons favours a model for the Myra Falls pyrite-rich horizons other than our proposed veinlet model for gold enrichment.

The proposed model of gold-bearing veinlets in emergent VMS systems has some implications for exploration as there may be subtle gold enrichments not yet identified in VMS systems that display continued development into shallower and shallower water systems, especially those with evidence of the sub-aqueous to sub-aerial transition.

ACKNOWLEDGEMENTS

Financial support for part of this project was provided by NSERC and Nyrstar grants to DM. Thanks are due Nyrstar staff, especially Lorri Cummings, for invaluable assistance with underground and drill core sampling, and access to the mine's geochemical database. Two very thorough reviews by ?? and ?? greatly improved an earlier version of this manuscript.

AUTHOR CONTRIBUTIONS

Conceptualization, Daniel Marshall and Rick Sawyer; Data curation, Daniel Marshall, Carol-Anne Nicol, Robert Greene, Armond Stansell and Ross Easterbrook; Formal analysis, Daniel Marshall, Carol-Anne Nicol and Robert Greene; Funding acquisition, Daniel Marshall and Rick Sawyer; Investigation, Daniel Marshall, Carol-Anne Nicol, Armond Stansell and Ross Easterbrook; Methodology, Daniel Marshall, Carol-Anne Nicol, Robert Greene and Armond Stansell; Project administration, Daniel Marshall and Rick Sawyer; Resources, Ross Easterbrook; Supervision, Daniel Marshall; Validation, Robert Greene, Armond Stansell and Ross Easterbrook; Writing – original draft, Daniel Marshall; Writing – review & editing, Daniel Marshall, Carol-Anne Nicol and Armond Stansell.

REFERENCES

1. Galley, A.G.; Hannington, M.D.; Jonasson, I.R.Volcanogenic massive sulphide deposits. In *Mineral Deposits of Canada: A Synthesis of Major Deposit-Types, District Metallogeny, the Evolution of Geological Provinces, and Exploration Methods*, Goodfellow, W.D., Ed.; Geological Association of Canada, Mineral Deposits Division: St. John's, NL, Canada, 2007; Special Publication No. 5, pp. 141-161.

2. Nyrstar Annual Report 2016. Available online: https://www.nyrstar.com/~/media/Files/N/Nyrstar/shareholder-meetings/english/2017/10-nyrstar-2016-annual-report-english-.pdf (accessed on 07 September 2018).

3. Huston, D.L. Gold in volcanic-hosted massive sulfide deposits: distribution, genesis, and exploration. *Rev. Econ. Geol.* **2000**, *13*, pp. 401-426.

4. Huston, D.L.; Large, R. A chemical model for the concentration of gold in volcanogenic massive sulphide deposits. *Ore Geol. Rev.* **1989**, *4*, pp. 171-200; DOI: 10.1016/0169-1368(89)90017-6.

5. Hannington, M.D.; Scott, S. Sulfidation equilibria as guides to gold mineralization in volcanogenic massive sulfides: evidence from sulfide mineralogy and the composition of sphalerite. *Econ. Geol. Bull. Soc.* **1989**, *84*, pp. 1978-1995; DOI: 10.2113/gsecongeo.84.7.1978.

6. Huston, D.L.; Bottrill, R.S.; Creelman, R.A.; Zaw, K.; Ramsden, T.R.; Rand, S.W.; Gemmell, J.B.; Jablonski, W.; Sie, S.H.; Large, R.R. Geologic and geochemical controls on the mineralogy and grain size of gold-bearing phases, eastern Australian volcanic-hosted massive sulfide deposits. *Econ. Geol.* **1992**, *87*, pp. 542-563; DOI: 10.2113/gsecongeo.87.3.542.

7. Jones, S.; Gemmell, J.B.; Davidson, G.J.; Petrographic, geochemical, and fluid inclusion evidence for the origin of siliceous cap rocks above volcanic-hosted massive sulfide deposits at Myra Falls, Vancouver Island, British Columbia, Canada. *Econ. Geol. Bull. Soc.* **2006**, *101*, pp. 555-584; DOI: 10.2113/gsecongeo.101.3.555.

8. Jones, S.; Berry, R.; Sinclair, B. Multiple deformation episodes at Myra Falls volcanic-hosted massive sulfide camp, central Vancouver Island, British Columbia, Canada. *Can. J. Earth Sci.* **2006**, *43*, pp. 1711-1732; DOI: 10.1139/E06-050.

9. Chong, A.; Becherer, M.; Sawyer, R.; Wastenays, H.; Baldwin, R.; Bakker, F.; McWilliams, I. *Massive sulphide deposits at Myra Falls operations, Vancouver Island, British Columbia*. BC Ministry of Energy, Mines and Petroleum Resources; 2005; GeoFile 2006-7.

10. Barrett, T.J.; Sherlock, R.L. Volcanic stratigraphy, lithogeochemistry and seafloor setting of the H-W massive sulfide deposit, Myra Falls, Vancouver Island, British Columbia. *Explor. Min. Geol.* **1996**, *5*, pp. 421-458.

11. Goldstein, R. Petrographic analysis of fluid inclusions. In *Fluid Inclusions: Analysis and Interpretation*; Samson, I., Anderson, A., Marshall, D., Eds.; Mineralogical Association of Canada: Ottawa, ON, Canada, 2003; Volume 32, pp. 9-53, ISBN 0921294328.

12. Kruger, Y.; Stoller, P.; Ricka, J.; Frenz, M. Femtosecond lasers in fluid-inclusion analysis: overcoming metastable phase states. *Eur. J. Mineral.* **2007**, *19*, pp. 693-706; DOI: 10.1127/0935-1221/2007/0019-1762.

13. Bodnar, R.J. Introduction to aqueous-electrolyte fluid inclusions. In *Fluid Inclusions: Analysis and Interpretation*; Samson, I.; Anderson, A., Marshall, D., Eds.; Mineralogical Association of Canada: Ottawa, ON, Canada, 2003; Volume 32, pp. 81-100; ISBN 0921294328.

14. Nelson, K.H.; Thompson, T.G. Deposition of salts from seawater by frigid concentration. *J. Marine Res.* **1954**, *13*, pp. 165-182.

15. Crawford, M.L. Phase equilibria in aqueous fluid inclusions. In *Fluid Inclusions: Applications to Petrology*; Hollister, L.S., Crawford, M.L., Eds.; Mineral Association of Canada: Ottawa, Canada, 1981; Volume 6, pp. 75-100.

16. Butterfield, D.A.; Massoth, G.J.; McDuff, R.E.; Lupton, J.E.; Lilley, M.D. Geochemistry from hydrothermal fluids from Axial Seamount Hydrothermal Emissions Study vent field, Juan

de Fuca Ridge: subseafloor boiling and subsequent fluid-rock interaction. *J. Geophys. Res.* **1990**, *95*, pp. 12895-12921; DOI: 10.1029/JB095iB08p12895.

17. Hannington, M.D.; Bleeker, W.; Kjarsgaard, I. Sulfide mineralogy, geochemistry and ore genesis of the Kidd Creek deposit: part II. The bornite zone. In *The Giant Kidd Creek Volcanogenic Massive Sulfide Deposit, Western Abitibi Subprovince, Canada*, Hannington, M.D., Barrie, C.T., Eds.; Economic Geology Monograph **1999**, *10*, pp. 225-266.

18. Hannington, M.D.; Poulsen, K.H.; Thompson, J.F.H.; Sillitoe, R.H. Volcanogenic gold in the massive sulfide environment. *Rev. Econ. Geol.* **1997**, *8*, pp. 325-356.

19. Heinrich, C.A.; Driesner, T.; Stefánsson, A.; Seward, T.M. Magmatic vapour contraction and transport of gold from the porphyry environment to epithermal ore deposits. *Geology* **2004**, *32*, pp. 761–764; DOI: 10.1130/G20629.1.

20. Monecke, T.; Petersen, S.; Hannington, M.D. Constraints on water depth of massive sulfide formation: evidence from modern seafloor hydrothermal systems in arc-related settings. *Econ. Geol.* **2014**, 109, pp. 2079–2101; DOI: 10.2113/econgeo.109.8.2079.

21. Nadaraju, G. Triassic-Jurassic biochronology of the Iskut River map areas, northwestern British Columbia. Unpublished M.Sc. thesis, University of British Columbia, Vancouver, Canada, 1993.

22. Sherlock, R.; Roth, T.; Spooner, E.; Bray, C. Origin of the Eskay Creek precious metal-rich volcanogenic massive sulfide deposit: fluid inclusion and stable isotope evidence. *Econ. Geol.* **1999**, *94*, pp. 803-824; DOI: 10.2113/gsecongeo.94.6.803.